UC Davis
UC Davis Previously Published Works

Title

The Effect of Bi-Terminal PEGylation of an Integrin αvβ6–Targeted 18F Peptide on Pharmacokinetics and Tumor Uptake

Permalink

https://escholarship.org/uc/item/79h4325h

Journal

Journal of Nuclear Medicine, 56(5)

ISSN

0161-5505

Authors

Hausner, Sven H
Bauer, Nadine
Hu, Lina Y
et al.

Publication Date

2015-05-01

DOI

10.2967/jnumed.114.150680

Peer reviewed

The Effect of Bi-Terminal PEGylation of an Integrin $\alpha_v\beta_6$–Targeted [18]F Peptide on Pharmacokinetics and Tumor Uptake

Sven H. Hausner[1,2], **Nadine Bauer**[2], **Lina Y. Hu**[2], **Leah M. Knight**[1], and **Julie L. Sutcliffe**[1,2,3,4]

[1]Division of Hematology/Oncology, Department of Internal Medicine, University of California Davis, Sacramento, California

[2]Department of Biomedical Engineering, University of California Davis, Davis, California

[3]Center for Molecular and Genomic Imaging, University of California Davis, Davis, California

[4]Radiochemistry Research and Training Facility, University of California Davis, Sacramento, California

Abstract

Radiotracers based on the peptide A20FMDV2 selectively target the cell surface receptor integrin $\alpha_v\beta_6$. This integrin has been identified as a prognostic indicator correlating with the severity of disease for several challenging malignancies. In previous studies of A20FMDV2 peptides labeled with 4-^{18}F-fluorobenzoic acid (^{18}F-FBA), we have shown that the introduction of poly(ethylene glycol) (PEG) improves pharmacokinetics, including increased uptake in $\alpha_v\beta_6$-expressing tumors. The present study evaluated the effect of site-specific C-terminal or dual (N- and C-terminal) PEGylation, yielding ^{18}F-FBAA20FMDV2-PEG$_{28}$ (**4**) and ^{18}F-FBA-PEG$_{28}$-A20FMDV2-PEG$_{28}$ (**5**), on $\alpha_v\beta_6$-targeted tumor uptake and pharmacokinetics. The results are compared with ^{18}F-FBA–labeled A20FMDV2 radiotracers (**1–3**) bearing either no PEG or different PEG units at the N terminus.

Methods—The radiotracers were prepared and radiolabeled on solid phase. Using 3 cell lines, DX3puroβ6 ($\alpha_v\beta_6$ +), DX3puro ($\alpha_v\beta_6$ −), and BxPC-3 ($\alpha_v\beta_6$ +), we evaluated the radiotracers in vitro (serum stability; cell binding and internalization) and in vivo in mouse models bearing paired DX3puroβ6–DX3puro and, for **5**, BxPC-3 xenografts.

Results—The size and location of the PEG units significantly affected $\alpha_v\beta_6$ targeting and pharmacokinetics. Although the C-terminally PEGylated **4** showed some improvements over the un-PEGylated ^{18}F-FBA-A20FMDV2 (**1**), it was the bi-terminally PEGylated **5** that displayed the more favorable combination of high $\alpha_v\beta_6$ affinity, selectivity, and pharmacokinetic profile. In vitro, **5** bound to $\alpha_v\beta_6$-expressing DX3puroβ6 and BxPC-3 cells with 60.5% ± 3.3% and 48.8% ± 8.3%, respectively, with a significant fraction of internalization (37.2% ± 4.0% and 37.6% ± 4.1% of total radioactivity, respectively). By comparison, in the DX3puro control **5** showed only 3.0% ± 0.5% binding and 0.9% ± 0.2% internalization. In vivo, **5** maintained high, $\alpha_v\beta_6$-directed binding

in the paired DX3puroβ6– DX3puro model (1 h: DX3puroβ6, 2.3 ± 0.2 percentage injected dose per gram [%ID/g]; DX3puroβ6/DX3puro ratio, 6.5:1; 4 h: 10.7:1). In the pancreatic BxPC-3 model, uptake was 4.7 ± 0.9 %ID/g (1 h) despite small tumor sizes (20–80 mg).

Conclusion—The bi-PEGylated radiotracer **5** showed a greatly improved pharmacokinetic profile, beyond what was predicted from individual N- or C-terminal PEGylation. It appears that the 2 PEG units acted synergistically to result in an improved metabolic profile including high $\alpha_v\beta_6$ + tumor uptake and retention.

Keywords

Integrins are heterodimeric transmembrane glycoprotein receptors composed of 2 noncovalently joint subunits, α and β. Only certain combinations between the known 18 α and 8 β subunits are formed, resulting in 24 integrins (1–3). Together, the integrin family of cell surface receptors is involved in cell binding, motility, and bidirectional signaling. Among the arginine-glycineaspartic acid (RGD)–recognizing group, the integrin $\alpha_v\beta_3$ has received much attention because of its role in angiogenesis, wound healing, and tumor metastasis (4–6). More recently, the integrin $\alpha_v\beta_6$ has become the focus of intense investigations where it was found to be involved in the production of cancer-promoting matrix metalloproteinases and tumor growth factor β and in the facilitation of the epithelial-mesenchymal transition (7–9). Although expression levels are generally undetectable in healthy adult tissues, clinical studies found that $\alpha_v\beta_6$ expression is highly upregulated in malignancies including pancreatic, basal cell, cervical, gastric, colorectal, and non–small cell lung cancer and oral squamous cell carcinoma (10–17). Frequently, increased expression levels have been found to correlate with poor prognosis, making integrin $\alpha_v\beta_6$ an important prognostic marker.

Peptides targeting the integrin $\alpha_v\beta_6$ have been derived from 1-bead-1-compound (18), phage-display (17,19–22), and yeast-display (23) library screening as well as from fragments of naturally occurring protein ligands (24–26). From these studies, which identified peptides with 7–20 amino acid residues, a consensus is emerging that the 7-residue RG/TDLXXL sequence (X = unspecified α-amino acid) describes a minimum motif generally advantageous for high affinity and selectivity toward $\alpha_v\beta_6$ and that additional flanking amino acids help in further improving these characteristics (19,27). When the unmodified initial lead compounds were analyzed in vitro, they oftentimes already possessed good binding affinities toward integrin $\alpha_v\beta_6$ (low nanomolar half maximal inhibitory concentration), but they performed poorly in vivo, largely because of rapid excretion, metabolic breakdown, or trapping in nontarget organs (23,28). Therefore, with the goal of achieving pharmacokinetic properties required for viable molecular imaging probes, modifications such as multimerization (29), cyclization (20), grafting onto scaffolds (23), and attachment of biocompatible polymers (28) are being pursued.

The 20-amino-acid peptide A20FMDV2 (sequence NAVPNLRGDLQVLAQKVART), derived from an envelope protein of the foot-and-mouth disease virus (FMDV), has been a focus of our studies (24–26). When the N-terminally 4-^{18}F-fluorobenzoyl (^{18}F-FBA)–

radiolabeled ^{18}F-FBA-A20FMDV2 (**1**; Fig. 1) was evaluated in mice, an uptake of 0.66 ± 0.09 and 0.69 ± 0.19 percentage injected dose per gram (%ID/g) at 1 h was found in $\alpha_v\beta_6$-expressing DX3puroβ6 melanoma and BxPC-3 pancreatic adenocarcinoma cell xenograft tumors, respectively, whereas 0.21 ± 0.07 %ID/g was observed for the $\alpha_v\beta_6$-negative DX3puro control (26,28). This first-generation radiotracer showed rapid washout from the $\alpha_v\beta_6$-expressing tumors and was degraded into 3 urine metabolites. We subsequently found that short, monodisperse poly(ethylene glycol) (PEG) units at the N terminus improved uptake to 1.9 ± 0.4 and 1.6 ± 0.3 %ID/g, respectively, for mono-PEGylated ^{18}F-FBA-PEG$_{28}$-A20FMDV2 (**2**) and di-PEGylated ^{18}F-FBA-(PEG$_{28}$)$_2$-A20FMDV2 (**3**) in BxPC-3 tumors at 1 h (28). Additionally, PEGylation suppressed washout from tumors and aided with stability; simultaneously, however, it also resulted in increased renal uptake and, for the di-PEGylated **3**, in renal trapping.

Here, in an effort to further investigate the effect of PEGylation on $\alpha_v\beta_6$-directed tumor targeting and improve the pharmacokinetic profile of A20FMDV2-derived radiotracers we investigated 2 different PEGylation patterns: C-terminally PEGylated ^{18}F-FBA-A20FMDV2- PEG$_{28}$ (**4**) and bi-terminally PEGylated ^{18}F-FBA-PEG$_{28}$-A20FMDV2- PEG$_{28}$ (**5**). The compounds were evaluated in vitro (serum stability, cell binding, and internalization) and in vivo (DX3puroβ6/DX3puro and BxPC-3 mouse models) and compared with the previously studied radiotracers.

MATERIALS AND METHODS

Chemistry and Radiochemistry

Peptide synthesis and radiolabeling were done on solid phase (30), and the radiotracer was formulated in phosphate-buffered saline using reagents described in the supplemental information (supplemental materials are available at http://jnm.snmjournals.org).

In Vitro Studies

Radiotracer affinity to and internalization into DX3puroβ6, DX3puro, and BxPC-3 cells were determined as previously described (30,31). To evaluate serum stability, mouse serum (0.5 mL) was combined with the radiotracer (12.5 μL; 0.74 MBq) and kept at 37°C (31,32). After precipitation of serum proteins (ethanol), the percentage of intact radiotracer was determined by high-performance liquid chromatography (HPLC).

Animal Studies

Female athymic nude mice (Charles River Laboratories) were handled following procedures approved by the University of California, Davis, Animal Use and Care Committee, and inoculated subcutaneously either with 3×10^6 DX3puro and 3×10^6 DX3puroβ6 cells on opposite flanks or with 3.5×10^6 BxPC-3 cells. Imaging was conducted once tumors had reached a maximum diameter of approximately 0.3–0.6 cm. The radiotracer (imaging, 6.5–9.0 MBq/animal; biodistribution, 1.1–2.0 MBq/animal) was injected intravenously into the tail of mice anesthetized with 2% isoflurane in oxygen.

For imaging studies, 2 animals per scan were placed side by side in a feet-first, prone position ($n = 4$ total/tumor model/radiotracer; anesthesia, 1.5%–2.0% isoflurane). PET/CT scans (dynamic 4×15-min PET emission scan starting 15 min after injection, single-frame 15-min PET emission scans at 2 and 4 h after injection) were acquired as previously described (31).

For biodistribution studies, the mice were anesthetized (4% isoflurane), sacrificed, and dissected ($n = 3$/time point/tumor model/radiotracer; 1, 2, and 4 h after injection). For blocking experiments, ^{19}F-FBA-PEG$_{28}$-A20FMDV2 (30 mg/kg, 10 mg/mL in saline) was injected intravenously ($n = 3$) 10 min before the radiotracer (28). Tissues were collected and rinsed and radioactivity measured in a γ counter (31). Calibrated, decay-corrected radioactivity concentrations are expressed as percentage injected dose per gram of sample (%ID/g). Urine was collected when possible; proteins were precipitated (ethanol) and supernatant aliquots analyzed by HPLC.

Tumor Autoradiography, Immunohistochemistry, and Radiotracer Stability in Tumor

After intravenous radiotracer injection (37 MBq/animal), tumor tissue was collected (1 h after injection), embedded in freezing medium, and sectioned (31). Autoradiography samples were exposed to a storage phosphor screen. For immunohistochemical $\alpha_v\beta_6$ staining, sections were fixed in a periodate–lysine–paraformaldehyde solution, treated with hydrogen peroxide/phosphate-buffered saline, incubated with anti-integrin β_6 antibody and a peroxidase-labeled secondary antibody (anti-goat-Ig), developed with 3,3′-diaminobenzidine, counterstained with Mayer hematoxylin (Poly Scientific), and mounted (DPX mounting medium [Electron Microscopy Sciences or Sigma Aldrich]).

To determine radiotracer stability, tumor tissue was collected 1 h after injection and homogenized, proteins precipitated (ethanol), and supernatant aliquots analyzed by HPLC (31).

RESULTS

Chemistry and Radiochemistry

Nonradioactive ^{19}F-**4** and ^{19}F-**5** were obtained in greater than 98% purity after HPLC purification: ^{19}F-**4**: MS (matrix-assisted laser desorption/ionization [MALDI]) m/z = 3587.5413 [M+H]$^+$, calcd M (C$_{159}$H$_{284}$FN$_{33}$O$_{57}$) 3587.0323; ^{19}F-**5**: MS (MALDI) m/z = 4891.2339 [M+H]$^+$, calcd M (C$_{218}$H$_{401}$FN$_{34}$O$_{86}$) 4890.8034. The corresponding ^{18}F radiotracers, prepared by solid-phase radiolabeling with ^{18}F-FBA (22.4 ± 4.1 GBq), were obtained in greater than 95% radiochemical purity (synthesis time, 137 ± 5 min; $n = 7$; Supplemental Fig. 1), with specific activities greater than 75 GBq/μmol and decay-corrected radiochemical yields of 14.9% ± 6.2% and 8.9% ± 1.4%, respectively, for **4** and **5**.

In Vitro Studies

Both radiotracers, ^{18}F-FBA-A20FMDV2-PEG$_{28}$ (**4**) and ^{18}F-FBA-PEG$_{28}$-A20FMDV2-PEG$_{28}$ (**5**), were stable in phosphate-buffered saline (4 h); in mouse serum 76% and 80% remained intact, respectively, after 60 min at 37°C. Both radiotracers showed high $\alpha_v\beta_6$-

targeted binding to and internalization into cells (Fig. 2): 32% ± 5% of **4** bound to DX3puroβ6 and 25% ± 3% to BxPC-3, whereas 4.5% ± 0.5% bound to the DX3puro control; for both $\alpha_v\beta_6$-expressing cell lines 13% (of total radioactivity) was internalized. By comparison, for **5** binding to $\alpha_v\beta_6$-expressing cells was nearly twice as high (DX3puroβ6, 61% ± 3%; BxPC-3, 49% ± 8%) and internalization tripled to 37% ± 4% and 38% ± 4%, respectively; for the DX3puro control binding and internalization remained low (3%).

The resulting uptake ratio for the DX3puroβ6–DX3puro pair was 7.1:1 for radiotracer **4** ($P = 3 \times 10^{-5}$) and 20:1 for radiotracer **5** ($P = 9 \times 10^{-7}$), and the corresponding internalization ratios were 9.4:1 and 41:1, respectively ($P = 0.0001$ and 8×10^{-5}).

In Vivo Studies

The 2 new radiotracers, **4** and **5**, were evaluated in the paired DX3puroβ6–DX3puro tumor model (Figs. 3 and 4; Table 1). ^{18}FFBA-A20FMDV2-PEG$_{28}$ (**4**) was well retained in the $\alpha_v\beta_6$- expressing DX3puroβ6 tumor for the first 2 h (1 h, 1.3 ± 0.3 %ID/g; 2 h, 1.0 ± 0.01 %ID/g) but then dropped to 0.27 ± 0.07 %ID/g at 4 h; uptake in the $\alpha_v\beta_6$-negative DX3puro tumor was 0.46 ± 0.13 %ID/g at 1 h, dropping to 0.11 ± 0.02 %ID/g at 4 h. The DX3puroβ6 tumor–to–DX3puro tumor ratios were greater than 2.5:1, and DX3puroβ6 tumor–to–blood ratios were greater than 2:1 throughout (both P 0.02; Fig. 3B). Uptake of ^{18}F-FBA-PEG$_{28}$-A20FMDV2-PEG$_{28}$ (**5**) in the DX3puroβ6 tumor was 2.3 ± 0.2 %ID/g at 1 h, before stabilizing at 1.4 ± 0.2 %ID/g (2 and 4 h); uptake in the $\alpha_v\beta_6$-negative DX3puro tumor was 0.39 ± 0.12 %ID/g at 1 h, dropping to 0.14 ± 0.04 %ID/g at 4 h. DX3puroβ6 tumor size did not affect radiotracer uptake, and even tumors weighing less than 50 mg were reliably detected (Supplemental Fig. 5). DX3puroβ6 tumor–to–DX3puro tumor ratios were greater than 6.0:1, and DX3puroβ6 tumor–to–blood ratios were greater than 4.5:1 throughout for radiotracer **5** (both P 0.001; Fig. 4B).

Renal clearance was the major route of elimination for both radiotracers. ^{18}F-FBA-A20FMDV2-PEG$_{28}$ (**4**) showed modest kidney uptake of 17 ± 2 %ID/g at 1 h, dropping to 2.1 ± 0.4 %ID/g at 4 h. Kidney uptake of ^{18}F-FBA-PEG$_{28}$-A20FMDV2-PEG$_{28}$ (**5**) was higher (67 ± 12 %ID/g at 1 h) but also dropped over time (19 ± 2 %ID/g at 4 h). Other organs with elevated levels of radioactivity for both radiotracers were the gallbladder, stomach, and intestine (all < 15 %ID/g at 1 h, dropping over time), indicating possible partial clearing via the hepatobiliary route. Muscle uptake was 1.0%–1.6 %ID/g (**4**) and 0.9 %ID/g (**5**) and lung uptake approximately 2–3 %ID/g (both radiotracers, all time points).

HPLC analysis of radioactivity extracted from DX3puroβ6 tumor revealed that for **4**, half of the radioactivity eluted metabolized with a short retention time (Supplemental Fig. 3), whereas for **5** the HPLC showed less than 20% apparent breakdown (Supplemental Fig. 4). HPLC of urine samples revealed 3 radioactive metabolites with short retention times for **4**, whereas for **5** the HPLC showed only a minor new peak (18%) possessing a slightly longer retention time (Supplemental Fig. 2).

Because of the better overall pharmacokinetic profile, ^{18}F-FBA-PEG$_{28}$-A20FMDV2-PEG$_{28}$ (**5**) was chosen for further evaluation in a pancreatic BxPC-3 mouse model (Fig. 4; Table 1). Here, a tumor uptake of 4.7 ± 0.9 %ID/g was observed at 1 h, dropping slightly to 4.1 ± 1.4

%ID/g (2 h) and 3.4 ± 1.3 %ID/g (4 h); tumor uptake could be reduced by 92% to 0.38 ± 0.05 %ID/g (1 h; $P = 0.001$) by preadministration of $\alpha_v\beta_6$-targeted blocking peptide. Low uptake in the pancreas (0.46 ± 0.07 %ID/g at 1 h, 0.25 ± 0.07 %ID/g at 4 h) resulted in BxPC-3–to–pancreas ratios of 9:1 or greater ($P < 0.01$); as shown in Figure 4C, BxPC-3–to–muscle ratios were around 4 to 5:1 ($P < 0.04$), whereas BxPC-3–to–blood and BxPC-3–to–liver ratios reached greater than 20:1 at 4 h (both: $P = 0.01$). These higher ratios resulted in clearly identifiable tumors by small-animal PET imaging at 1, 2, and 4 h (Fig. 5A); the only other notable organs were the kidneys, bladder (urine), gallbladder, and the gastrointestinal tract. HPLC of radio-activity extracted from the tumor 1 h after injection revealed less than 20% apparent breakdown (Supplemental Fig. 4) and autoradiography of BxPC-3 xenograft slices showed the most pronounced uptake of radioactivity in the rim of the tumors in areas shown by immunohistochemistry to express integrin $\alpha_v\beta_6$ (Fig. 5B).

DISCUSSION

Since its discovery in pancreatic cancer (33), increasing data from molecular biology and clinical studies point to the epithelial cell surface receptor integrin $\alpha_v\beta_6$ as a potentially important diagnostic and therapeutic target of many challenging cancers, including pancreatic cancer (7–17,34). To that end, several $\alpha_v\beta_6$-specific peptide ligands, sharing a 7-residue RG/TDLXXL core motif (X = unspecified α-amino acid), have been identified and used in preclinical imaging studies (17,19–23,26–28,35,36). Among them, the 20-amino-acid peptide A20FMDV2 (24–26,37) has excellent affinity and selectivity for the integrin $\alpha_v\beta_6$ and provides a good platform for the development of imaging probes, particularly when radiolabeled with ^{18}F (26,28,30). In vitro studies showed the beneficial effects of PEGylation on $\alpha_v\beta_6$-targeted cell binding and internalization (Fig. 2); specifically, adding 1 PEG_{28} unit at the N terminus (**2**) or, as shown in the present study, 1 PEG_{28} unit each at the N terminus and C terminus (**5**) gave the best results (>45% of total radioactivity bound to $\alpha_v\beta_6$-positive cell, and >60% of bound radioactivity internalized). By comparison, adding 1 PEG_{28} unit at the C terminus (**4**) or 2 at the N terminus (**3**) resulted in smaller improvements (approximately half of those seen for **2** and **5**). Regardless of PEGylation pattern, binding to the $\alpha_v\beta_6$-negative control DX3puro cells remained low (<5% of total radioactivity). Because both DX3 cell lines express similar levels of other RGD-directed integrins, including $\alpha_v\beta_3$, $\alpha_v\beta_5$, $\alpha_v\beta_8$, and $\alpha_5\beta_1$ (26), these results confirm that the increased affinity of the PEGylated radiotracers did not diminish the high selectivity for integrin $\alpha_v\beta_6$. Still, even for promising lead compounds identified in vitro (**2** and **5**), it is important to carefully evaluate their potential as imaging probes in vivo, where other, complex pharmacokinetic and metabolic factors come into play.

Beneficial in vivo effects of PEGylation (38) on stability, pharmacokinetics, and tumor uptake and retention have previously been described for other PET radiotracers, for example, the integrin $\alpha_v\beta_3$–targeting cyclo-RGD peptides (39). Similarly, we found significant in vivo effects of PEGylation on tumor-targeting and pharmacokinetics: although the unmodified ^{18}F-FBA-A20FMDV2 (**1**) did show $\alpha_v\beta_6$-targeted tumor uptake, it also suffered from washout (BxPC-3 model, 0.69 ± 0.19 %ID/g at 1 h, 0.12 ± 0.03%ID/g at 4 h (28)) and metabolic breakdown (Supplemental Fig. 2). N-terminal incorporation of 1 or 2 PEG_{28} units significantly increased tumor uptake and retention (BxPC-3 model, 1.5 ± 0.04

and 2.1 ± 0.4 %ID/g at 4 h for **2** and **3**, respectively (28)) and reduced the number of metabolites found in urine (Fig. 1; Supplemental Fig. 2); unfortunately, it came at a cost of increased kidney uptake and retention (when 2 PEG units were introduced [**3**]; Table 1).

The incorporation of PEG_{28} at the C terminus demonstrated the position-sensitivity of PEGylation with respect to pharmacokinetics: ^{18}F-FBA-PEG_{28}-A20FMDV2 (**2**) had a steady tumor uptake of 0.5 ± 0.1 %ID/g (DX3puroβ6, 1 and 4 h (28)); by contrast, ^{18}F-FBA-A20FMDV2-PEG_{28} (**4**) had higher tumor uptake early on, followed by washout (DX3puroβ6, 1.3 ± 0.3 %ID/g at 1 h to 0.27 ± 0.07 %ID/g at 4 h; Fig. 3). Both **2** and **4** showed identical renal clearance (Table 1), but whereas HPLC of urine indicated 1 main metabolite for **2**, 3 metabolites were found for **4** (Supplemental Fig. 2). The latter pattern is similar to that seen for the unmodified ^{18}F-FBA-A20FMDV2 (**1**); together with the observed washout from tumor, these data indicate that C-terminal PEGylation conferred better tumor targeting but poorer protection from metabolic breakdown and washout from the $\alpha_v\beta_6$+ tumor.

Bi-terminal PEGylation further improved both DX3puroβ6 tumor uptake (**5**, 2.3 ± 0.2 %ID/g at 1 h) and retention (1.4 ± 0.2 %ID/g at 2 and 4 h), resulting in largely improved DX3puroβ6-totissue ratios for key tissues including the muscle, liver, and control DX3puro tumor; uptake in the latter was the same for **4** and **5** (Figs. 3 and 4; Table 1). A notable exception was the kidneys: their initial uptake increased (similar to the results obtained when adding a second PEG_{28} unit at the N terminus, i.e., going from **2** to **3**), but, unlike for **3**, the radioactivity did wash out over time (Table 1). Because expression of integrin $\alpha_v\beta_6$ in murine kidneys has been shown to be negligible (37,40), the renal retention of radiotracer is not target-mediated and can likely be improved by further modifications of the radiotracer. HPLC analysis of DX3puroβ6 tumor homogenates showed considerably less metabolic breakdown for **5** than for **4** (<20% vs. 50%); given this increased apparent stability and the promising biodistribution data, specifically the good retention in the DX3puroβ6 tumors and the DX3puroβ6- to-organ ratios, we were encouraged to evaluate **5** further in the BxPC-3 model, a human pancreatic carcinoma cell line that endogenously expresses the integrin $\alpha_v\beta_6$. Here, tumor uptake more than doubled, compared with the DX3puroβ6 model (Table 1), resulting in favorable tumor-to-organ ratios, including tumor to pancreas, 9:1 or greater, and tumor to muscle, 4 to 5:1 (Fig. 4). Importantly for the detection of early lesions, all tumors did show good radiotracer uptake, regardless of size (20–80 mg) or time point (Supplemental Fig. 5). This, along with the washout from healthy organs, resulted in clearly identifiable tumors in PET/CT images (Fig. 5); autoradiography and immunohistochemistry confirmed colocalization of radioactivity with areas of integrin $\alpha_v\beta_6$ expression, particularly in focal points at the rim of the tumor.

Besides A20FMDV2-derived radiotracers, several peptide-based PET and SPECT imaging probes for integrin $\alpha_v\beta_6$ are currently being evaluated in mouse models (27), among them the 36-amino-acid cystine knot peptides ^{18}F-fluorobenzoate-R_o1 and ^{64}Cu-DOTA-R_o1 (23,35) and versions of the phage-screening–derived TP H2009.1 (22) such as the 21-amino-acid ^{99m}Tc-HHK (36) and the dimerized 10-amino-acid ^{64}Cu-AcD10 (40). Supplemental Table 1 shows the peptide sequences. Although comparisons across different animal models and experimental protocols need to be approached with great caution, these studies

collectively offer a context for the current state of A20FMDV2-derived radiotracers and suggest avenues for further improvement of **5**: easily synthesized and radiolabeled on solid phase, **5** showed an $\alpha_v\beta_6$+ tumor uptake of 2.3 ± 0.2 %ID/g (DX3puroβ6, 1 h) and 4.7 ± 0.9 %ID/g (BxPC-3, 1 h), good $\alpha_v\beta_6$ + tumor retention, and a DX3puroβ6-to-DX3puro ratio of greater than 6:1. These results compare favorably with literature data, including 1-h tumor uptake (%ID/g; 0.52 [^{99m}Tc-HHK; BxPC-3], 1.46 [^{64}Cu-AcD10; H2009], ~2 [^{18}F-fluorobenzoate-R$_o$1; BxPC-3], 4.13 [^{64}Cu-DOTA-R$_o$1; BxPC-3]) and $\alpha_v\beta_6$+/$\alpha_v\beta_6^-$ tumor uptake ratios (~1.8:1 [^{18}F-fluorobenzoate-R$_o$1; BxPC-3/HEK-293] to 3.3:1 [^{99m}Tc-HHK; BxPC-3/HEK-293). For all of these radiotracers, including **5**, kidneys are the organ with the highest uptake (it is not target-mediated as the kidneys do not express integrin $\alpha_v\beta_6$ (37,40)) and the radiometalated compounds tend to show higher renal uptake and retention (as seen for ^{99m}Tc-HHK and ^{64}Cu-DOTA-R$_o$1); significant reductions in renal uptake and retention are possible through thoughtful modifications (as demonstrated for ^{64}Cu-AcD10 where the acetylation of the amine functionalities was responsible for a 75% reduction in kidney uptake to 5.4 ± 0.9 %ID/g 24 h after injection). Similarly, modifications to the peptide can also help with renal clearance of ^{18}F-labeled peptide radiotracers for integrin $\alpha_v\beta_6$ (28,35). We therefore are confident that the increased kidney uptake observed for ^{18}F-FBA-PEG$_{28}$-A20FMDV2-PEG$_{28}$ (**5**) can be mitigated by further modifications such as elimination of positively charged sites, multimerization (40), and introduction of carefully chosen steric restrictions (35) without negatively affecting $\alpha_v\beta_6$-targeted tumor uptake.

CONCLUSION

The radiotracers ^{18}F-FBA-A20FMDV2-PEG$_{28}$ (**4**) and ^{18}F-FBA-PEG$_{28}$-A20FMDV2-PEG$_{28}$ (**5**) were prepared and compared with other A20FMDV2 peptide–derived radiotracers. In vitro and in vivo studies showed that both size and location of the PEG units significantly affected $\alpha_v\beta_6$ targeting and pharmacokinetics. The bi-PEGylated radiotracer ^{18}F-FBA-PEG$_{28}$-A20FMDV2-PEG$_{28}$ in particular showed a greatly improved pharmacokinetic profile, beyond what was predicted from individual N- or C-terminal PEGylation, making it a lead candidate for further optimization and translational studies. To that end, work is currently under way to elucidate the metabolic fate and further improve the biodistribution profile.

Supplementary Material

Refer to Web version on PubMed Central for supplementary material.

ACKNOWLEDGMENTS

References

1. Hynes RO. Integrins: bidirectional, allosteric signaling machines. Cell. 2002; 110:673–687. [PubMed: 12297042]

2. Srichai, MN.; Zent, R. Integrin structure and function. In: Zent, R.; Pozzi, A., editors. Cell-Extracellular Matrix Interactions in Cancer. New York, NY: Springer; 2010. p. 19-41.

3. Takada Y, Ye X, Simon S. The integrins. Genome Biol. 2007; 8:215.1–215.9. [PubMed: 17543136]

4. Wadas TJ, Wong EH, Weisman GR, Anderson CJ. Coordinating radiometals of copper, gallium, indium, yttrium, and zirconium for PET and SPECT imaging of disease. Chem Rev. 2010; 110:2858–2902. [PubMed: 20415480]

5. Desgrosellier JS, Cheresh DA. Integrins in cancer: biological implications and therapeutic opportunities. Nat Rev Cancer. 2010; 10:9–22. [PubMed: 20029421]

6. Beer AJ, Schwaiger M. Imaging of integrin $\alpha_v\beta_3$ expression. Cancer Metastasis Rev. 2008; 27:631–644. [PubMed: 18523730]

7. Vogetseder A, Thies S, Ingold B, et al. α_v-Integrin isoform expression in primary human tumors and brain metastases. Int J Cancer. 2013; 133:2362–2371. [PubMed: 23661241]

8. Lu X, Lu D, Scully M, Kakkar V. The role of integrins in cancer and the development of anti-integrin therapeutic agents for cancer therapy. Perspect Medicin Chem. 2008; 2:57–73. [PubMed: 19787098]

9. Bandyopadhyay A, Raghavan S. Defining the role of integrin $\alpha_v\beta_6$ in cancer. Curr Drug Targets. 2009; 10:645–652. [PubMed: 19601768]

10. Li HX, Zheng JH, Fan HX, Li HP, Gao ZX, Chen D. Expression of $\alpha_v\beta_6$ integrin and collagen fibre in oral squamous cell carcinoma: association with clinical outcomes and prognostic implications. J Oral Pathol Med. 2013; 42:547–556. [PubMed: 23331428]

11. Sipos B, Hahn D, Carceller A, et al. Immunohistochemical screening for β_6-integrin subunit expression in adenocarcinomas using a novel monoclonal antibody reveals strong up-regulation in pancreatic ductal adenocarcinomas in vivo and in vitro. Histopathology. 2004; 45:226–236. [PubMed: 15330800]

12. Marsh D, Dickinson S, Neill GW, Marshall JF, Hart IR, Thomas GJ. $\alpha_v\beta_6$ Integrin promotes the invasion of morphoeic basal cell carcinoma through stromal modulation. Cancer Res. 2008; 68:3295–3303. [PubMed: 18451156]

13. Hazelbag S, Kenter GG, Gorter A, et al. Overexpression of the $\alpha_v\beta_6$ integrin in cervical squamous cell carcinoma is a prognostic factor for decreased survival. J Pathol. 2007; 212:316–324. [PubMed: 17503414]

14. Zhang ZY, Xu KS, Wang JS, et al. Integrin $\alpha_v\beta_6$ acts as a prognostic indicator in gastric carcinoma. Clin Oncol (R Coll Radiol). 2008; 20:61–66. [PubMed: 17981018]

15. Bates RC. Colorectal cancer progression: integrin $\alpha_v\beta_6$ and the epithelial-mesenchymal transition (EMT). Cell Cycle. 2005; 4:1350–1352. [PubMed: 16123591]

16. Yang SB, Du Y, Wu BY, et al. Integrin $\alpha_v\beta_6$ promotes tumor tolerance in colorectal cancer. Cancer Immunol Immunother. 2012; 61:335–342. [PubMed: 21913024]

17. Elayadi AN, Samli KN, Prudkin L, et al. A peptide selected by biopanning identifies the integrin $\alpha_v\beta_6$ as a prognostic biomarker for nonsmall cell lung cancer. Cancer Res. 2007; 67:5889–5895. [PubMed: 17575158]

18. Gagnon MKJ, Hausner SH, Marik J, Abbey CK, Marshall JF, Sutcliffe JL. High-throughput in vivo screening of targeted molecular imaging agents. Proc Natl Acad Sci USA. 2009; 106:17904–17909. [PubMed: 19815497]

19. Kraft S, Diefenbach B, Mehta R, Jonczyk A, Luckenbach GA, Goodman SL. Definition of an unexpected ligand recognition motif for $\alpha_v\beta_6$ integrin. J Biol Chem. 1999; 274:1979–1985. [PubMed: 9890954]

20. Hsiao JR, Chang Y, Chen YL, et al. Cyclic $\alpha_v\beta_6$-targeting peptide selected from biopanning with clinical potential for head and neck squamous cell carcinoma. Head Neck. 2010; 32:160–172. [PubMed: 19572290]

21. Nothelfer EM, Zitzmann-Kolbe S, Garcia-Boy R, et al. Identification and characterization of a peptide with affinity to head and neck cancer. J Nucl Med. 2009; 50:426–434. [PubMed: 19223422]

22. Oyama T, Sykes KF, Samli KN, Minna JD, Johnston SA, Brown KC. Isolation of lung tumor specific peptides from a random peptide library: generation of diagnostic and cell-targeting reagents. Cancer Lett. 2003; 202:219–230. [PubMed: 14643452]

23. Kimura RH, Teed R, Hackel BJ, et al. Pharmacokinetically stabilized cystine knot peptides that bind $\alpha_v\beta_6$ integrin with single-digit nanomolar affinities for detection of pancreatic cancer. Clin Cancer Res. 2012; 18:839–849. [PubMed: 22173551]

24. Logan D, Abughazaleh R, Blakemore W, et al. Structure of a major immunogenic site on foot-and-mouth-disease virus. Nature. 1993; 362:566–568. [PubMed: 8385272]

25. Jackson T, Sheppard D, Denyer M, Blakemore W, King AMQ. The epithelial integrin $\alpha_v\beta_6$ is a receptor for foot-and-mouth disease virus. J Virol. 2000; 74:4949–4956. [PubMed: 10799568]

26. Hausner SH, DiCara D, Marik J, Marshall JF, Sutcliffe JL. Use of a peptide derived from foot-and-mouth disease virus for the noninvasive imaging of human cancer: generation and evaluation of 4-^{18}F-fluorobenzoyl A20FMDV2 for in vivo imaging of integrin $\alpha_v\beta_6$ expression with positron emission tomography. Cancer Res. 2007; 67:7833–7840. [PubMed: 17699789]

27. Liu H, Wu Y, Wang F, Liu Z. Molecular imaging of integrin $\alpha_v\beta_6$ expression in living subjects. Am J Nucl Med Mol Imaging. 2014; 4:333–345. [PubMed: 24982819]

28. Hausner SH, Abbey CK, Bold RJ, et al. Targeted in vivo imaging of integrin $\alpha_v\beta_6$ with an improved radiotracer and its relevance in a pancreatic tumor model. Cancer Res. 2009; 69:5843–5850. [PubMed: 19549907]

29. Gray BP, McGuire MJ, Brown KC. A liposomal drug platform overrides peptide ligand targeting to a cancer biomarker, irrespective of ligand affinity or density. PLoS ONE. 2013; 8:e72938. [PubMed: 24009717]

30. Hausner SH, Kukis DL, Gagnon MKJ, et al. Evaluation of ^{64}Cu-DOTA and ^{64}Cu-CB-TE2A chelates for targeted positron emission tomography with an $\alpha v\beta 6$-specific peptide. Mol Imaging. 2009; 8:111–121. [PubMed: 19397856]

31. Hausner SH, Bauer N, Sutcliffe JL. In vitro and in vivo evaluation of the effects of aluminum ^{18}F-fluoride radiolabeling on an integrin $\alpha_v\beta_6$-specific peptide. Nucl Med Biol. 2014; 41:43–50. [PubMed: 24267053]

32. Gottumukkala V, Heinrich TK, Baker A, et al. Biodistribution and stability studies of ^{18}F-fluoroethylrhodamine B, a potential PET myocardial perfusion agent. Nucl Med Biol. 2010; 37:365–370. [PubMed: 20346876]

33. Sheppard D, Rozzo C, Starr L, Quaranta V, Erle DJ, Pytela R. Complete amino-acid-sequence of a novel integrin beta subunit (β_6) identified in epithelial-cells using the polymerase chain-reaction. J Biol Chem. 1990; 265:11502–11507. [PubMed: 2365683]

34. Yang G-Y, Xu K-S, Pan Z-Q, et al. Integrin $\alpha_v\beta_6$ mediates the potential for colon cancer cells to colonize in and metastasize to the liver. Cancer Sci. 2008; 99:879–887. [PubMed: 18294287]

35. Hackel BJ, Kimura RH, Miao Z, et al. ^{18}F-fluorobenzoate-labeled cystine knot peptides for PET imaging of integrin $\alpha_v\beta_6$. J Nucl Med. 2013; 54:1101–1105. [PubMed: 23670900]

36. Liu Z, Liu H, Ma T, et al. Integrin $\alpha_v\beta_6$-targeted SPECT imaging for pancreatic cancer detection. J Nucl Med. 2014; 55:989–994. [PubMed: 24711651]

37. Saha A, Ellison D, Thomas GJ, et al. High-resolution in vivo imaging of breast cancer by targeting the pro-invasive integrin $\alpha_v\beta_6$. J Pathol. 2010; 222:52–63. [PubMed: 20629113]

38. Harris JM, Chess RB. Effect of PEGylation on pharmaceuticals. Nat Rev Drug Discov. 2003; 2:214–221. [PubMed: 12612647]

39. Chen K, Conti PS. Target-specific delivery of peptide-based probes for PET imaging. Adv Drug Deliv Rev. 2010; 62:1005–1022. [PubMed: 20851156]

40. Singh AN, McGuire MJ, Li S, et al. Dimerization of a phage-display selected peptide for imaging of $\alpha_v\beta_6$-integrin: two approaches to the multivalent effect. Theranostics. 2014; 4:745–760. [PubMed: 24883124]
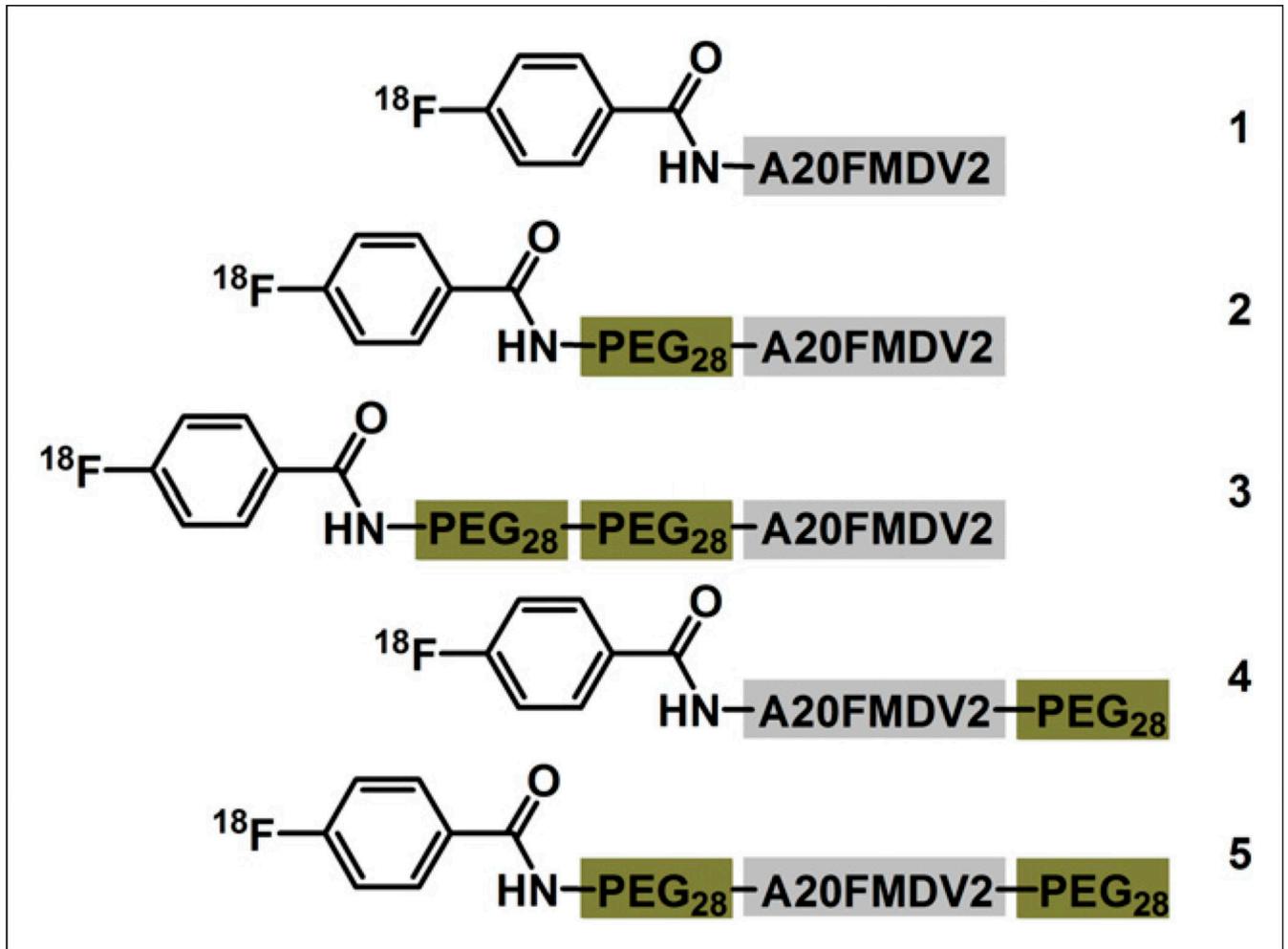
Figure 1.
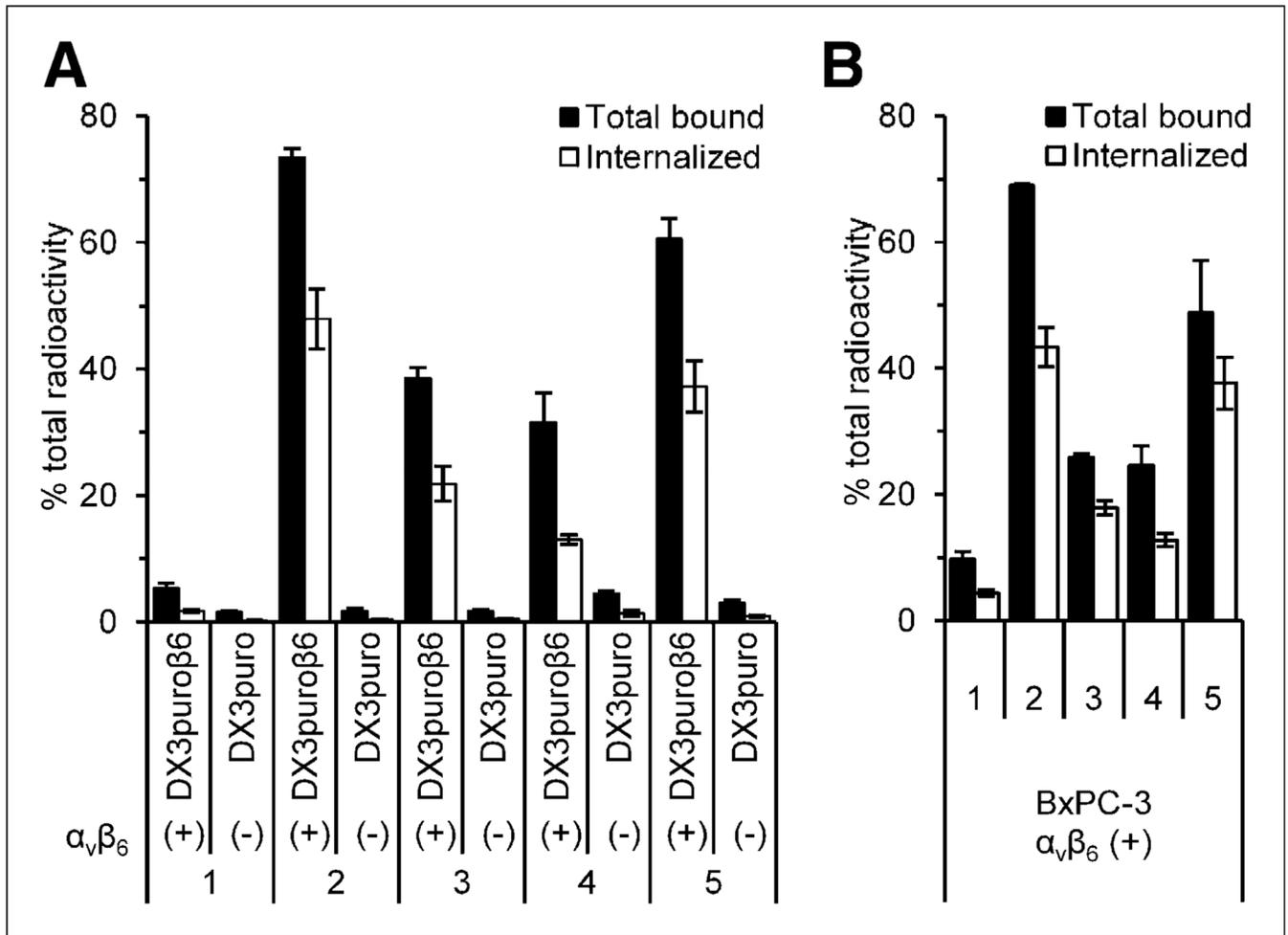Structures of radiotracers evaluated.

Figure 2.
Binding and internalization of radiotracers in vitro. (A) Paired, integrin $\alpha_v\beta_6$–expressing DX3puroβ6 cell line and non–$\alpha_v\beta_6$-expressing DX3puro control (P 0.0001 for corresponding data sets). (B) Integrin $\alpha_v\beta_6$–expressing BxPC-3 cell line. Filled columns = fraction of total radioactivity (n = 4/radiotracer/cell line/condition; 60 min); bars = SD. Data for **1–3** are from Hausner et al. (28).
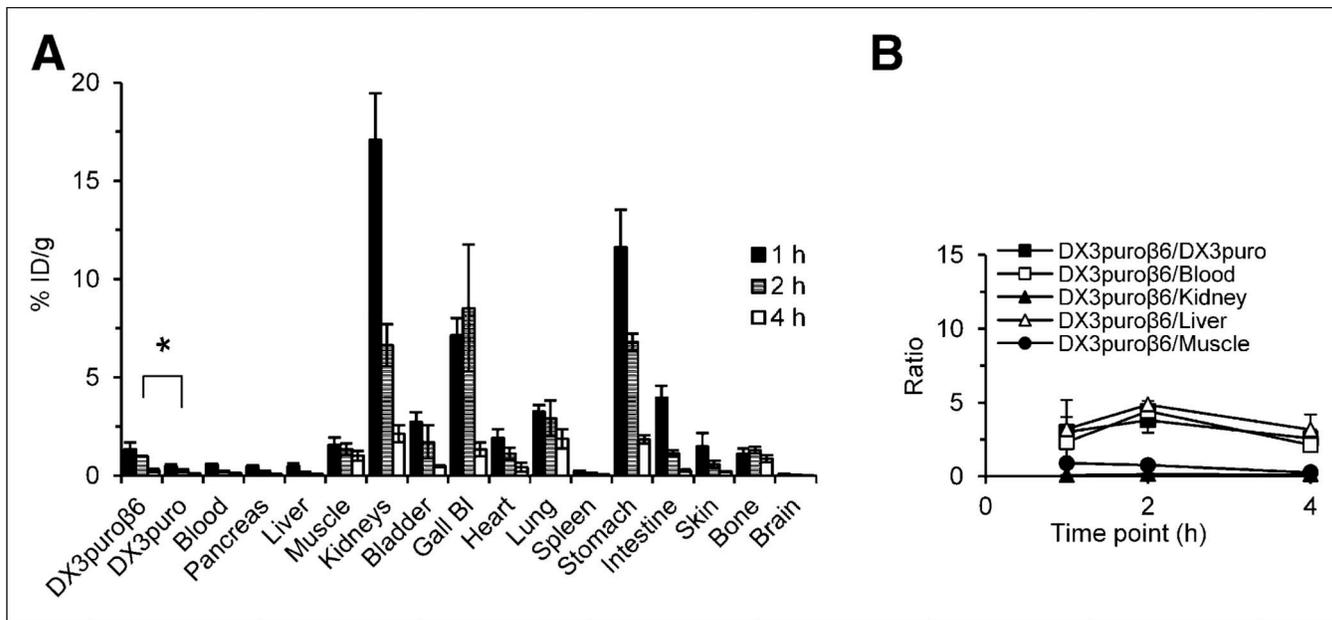
Figure 3.
Biodistribution data of ^{18}F-FBA-A20FMDV2-PEG$_{28}$ (**4**) in mice bearing paired $\alpha_v\beta_6$-expressing DX3puroβ6 and non–$\alpha_v\beta_6$-expressing DX3puro xenograft tumors. (A) Organ uptake (%ID/g; bars = SD; n = 3/time point). *P 0.02 for corresponding time points. (B) Uptake ratios of **4** for tumors and selected organs (bars = SD). Bl = bladder.
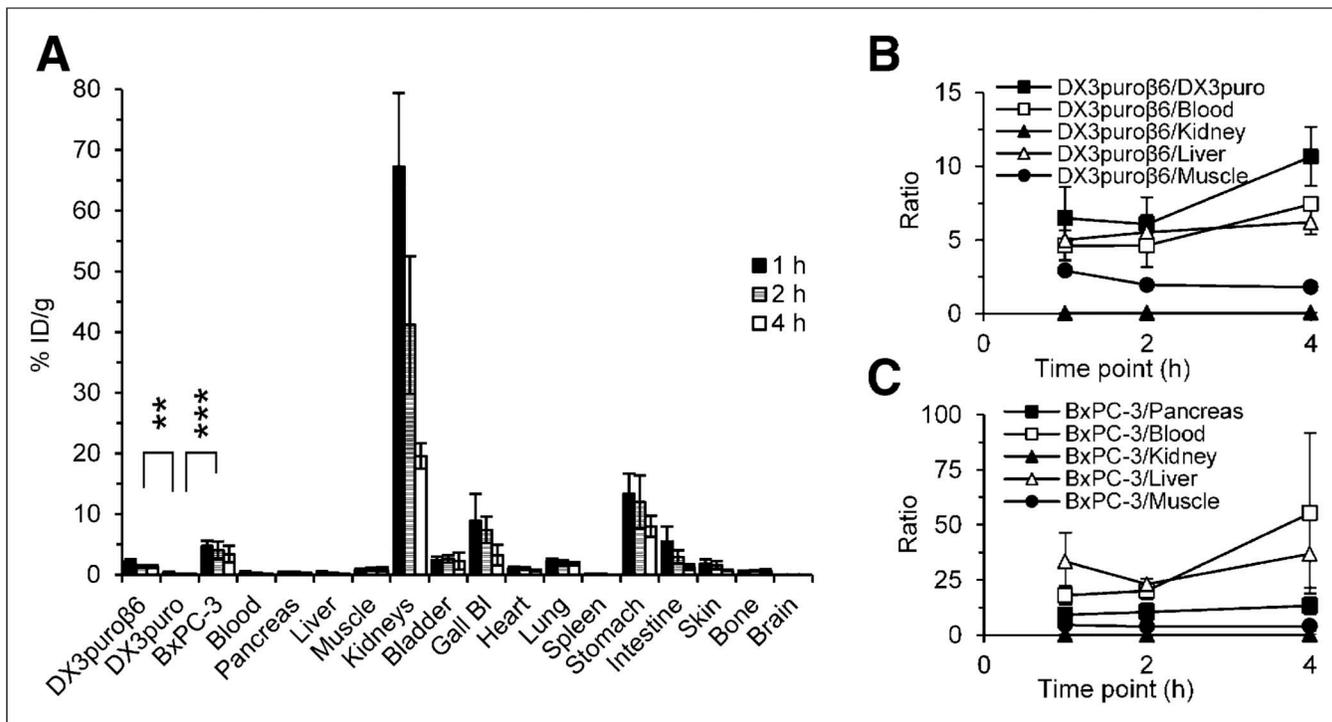
Figure 4.
Biodistribution data of ^{18}F-FBA-PEG$_{28}$-A20FMDV2-PEG$_{28}$ (**5**) in mice bearing either paired $\alpha_v\beta_6$-expressing DX3puroβ6 and non–$\alpha_v\beta_6$-expressing DX3puro xenograft tumors or $\alpha_v\beta_6$-expressing BxPC-3 xenograft tumors. (**A**) Organ uptake (%ID/g; bars = SD; tumors: n = 3/time point, nontumor tissues: n = 6/time point). **P 0.001 for corresponding time points. ***P 0.014 for corresponding time points. Uptake ratios of **5** for tumors and selected organs in paired DX3 tumor model (B) and BxPC-3 tumor model (C) (bars = SD). Bl = bladder.
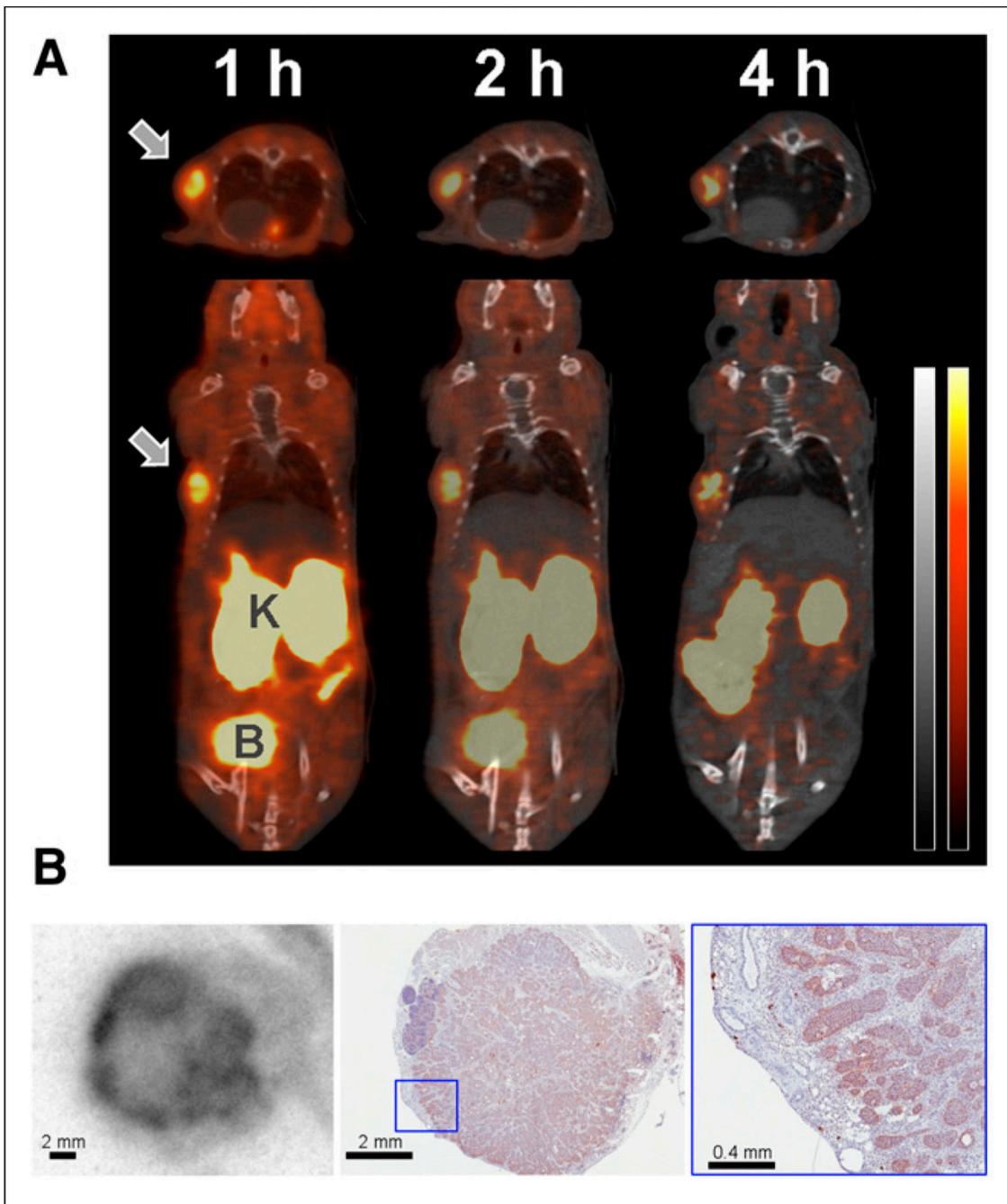
Figure 5.
(A) Representative transaxial and coronal cross-sections of PET/CT images obtained after injection of ^{18}F-FBA-PEG$_{28}$-A20FMDV2-PEG$_{28}$ (**5**; 8.9 MBq) in mouse bearing BxPC-3 xenograft (66 mg; arrow). CT is gray and PET red. B = Bladder; K = Kidneys. (B) Autoradiography image of BxPC-3 tumor harvested 1 h after injection of **5** (39 MBq; left) and matched adjacent immunohistochemistry slice stained for integrin $\alpha_v\beta_6$ expression (middle, right: magnified section).

TABLE 1

Radiotracer Uptake in Tumors and Selected Organs in Athymic Mouse Models

Radiotracer	Tissue[*]	1 h	2 h	4 h
1[†]	DX3puroβ6	0.66 ± 0.09	0.28 ± 0.03	0.06 ± 0.00
	DX3puro	0.21 ± 0.07	0.07 ± 0.02	0.02 ± 0.01
	BxPC-3	0.69 ± 0.19	0.32 ± 0.03	0.12 ± 0.03
	Kidney	3.3 ± 0.8	1.0 ± 0.8	0.16 ± 0.09
	Muscle	0.54 ± 0.18	0.30 ± 0.19	0.05 ± 0.02
	Blood	0.21 ± 0.07	0.07 ± 0.01	0.02 ± 0.01
2[†]	DX3puroβ6	0.49 ± 0.12	0.42 ± 0.05	0.49 ± 0.04
	DX3puro	0.10 ± 0.03	0.05 ± 0.00	0.07 ± 0.06
	BxPC-3	1.9 ± 0.4	1.3 ± 0.1	1.5 ± 0.04
	Kidney	19 ± 5	7.4 ± 1.8	3.3 ± 0.7
	Muscle	0.75 ± 0.47	0.58 ± 0.14	0.41 ± 0.09
	Blood	0.16 ± 0.02	0.05 ± 0.02	0.03 ± 0.03
3[†]	DX3puroβ6	0.52 ± 0.09	0.61 ± 0.11	0.54 ± 0.08
	DX3puro	0.11 ± 0.03	0.09 ± 0.03	0.06 ± 0.01
	BxPC-3	1.6 ± 0.3	2.3 ± 0.5	2.1 ± 0.4
	Kidney	43 ± 13	41 ±7	42 ± 5
	Muscle	0.38 ± 0.03	0.69 ± 0.03	0.47 ± 0.06
	Blood	0.18 ± 0.10	0.09 ± 0.02	0.01 ± 0.01
4[‡]	DX3puroβ6	1.3 ± 0.3	1.0 ± 0.01	0.27 ± 0.07
	DX3puro	0.46 ± 0.13	0.27 ± 0.06	0.11 ± 0.02
	Kidney	17 ± 2	6.6 ± 1.1	2.1 ± 0.4
	Muscle	1.6 ± 0.4	1.4 ± 0.3	1.0 ± 0.3
	Blood	0.57 ± 0.03	0.23 ± 0.02	0.12 ± 0.02
5	DX3puroβ6	2.3 ± 0.2	1.4 ± 0.2	1.4 ± 0.2
	DX3puro	0.39 ± 0.12	0.23 ± 0.01	0.14 ± 0.04
	BxPC-3	4.7 ± 0.9	4.1 ± 1.4	3.4 ± 1.3
	Kidney	67 ± 12	41 ± 11	19 ± 2
	Muscle	0.91 ± 0.16	0.90 ± 0.22	0.90 ± 0.33
	Blood	0.40 ± 0.16	0.26 ± 0.07	0.14 ± 0.07

[*] $\alpha_v\beta_6$- positive: DX3puroβ6, BxPC-3; $\alpha_v\beta_6$-negative: DX3puro.

[†] Data for 1–3 from Hausner et al. (26,28).

[‡] No BxPC-3 data collected.

Data determined by biodistribution and expressed as %ID/g ± SD (n = 3/time point/compound).